47th AIAA/ASME/SAE/ASEE Joint Propulsion Conference & Exhibit
31 July - 03 August 2011, San Diego, California

AIAA 2011-5953

Exact Solutions for the Integral Form of the Compressible Flowfield in a Porous Cylinder

Michel Akiki* and Joseph Majdalani†
University of Tennessee Space Institute, Tullahoma, TN 37388

In this article, analytical solutions for the compressible pressure field in an axisymmetric porous cylinder are developed assuming rotational, steady and inviscid conditions. The flow is driven by gaseous injection from the sidewall where an arbitrary velocity profile or mass flux may be imposed. The work constitutes an essential extension to a study in which the compressible equations of motion are reduced to a single integral equation, as shown by Akiki, M., and Majdalani, J., "Compressibility Effects in Slender Rocket Motors," AIAA Paper 2009-5326, August 2009. In this sequel, an Abel transform will be employed to solve the problem's characteristic integral equation directly for the pressure distribution, albeit at discrete ratios of specific heats. Other properties such as temperature, velocity, Mach number and density are then deduced throughout the domain. Our results are validated using comparisons to other analytical and numerical solutions to this problem. These are showcased against incompressible and one-dimensional theoretical formulations to explore their distinct differences. Finally, the capability of the present formulation to accommodate an arbitrarily prescribed sidewall injection configuration is leveraged to predict the flowfield induced by a spatially oscillatory injection profile.

Nomenclature

a	=	chamber radius
c_p	=	constant pressure specific heat
L_0	=	length of chamber
L_s	=	sonic length (critical distance)
M	=	Mach number
m	=	injection mass flux
P	=	nondimensional pressure
p	=	dimensional pressure
r	=	coordinate normal to the propellant surface
T	=	temperature
U_w	=	wall injection velocity
u	=	axial velocity
v	=	radial velocity
X	=	nondimensional axial coordinate
x	=	dimensional axial coordinate

Greek

ψ	=	stream function
χ	=	axial coordinate referenced to the sonic length, x / L_s
γ	=	ratio of specific heats
ρ	=	density
ξ	=	distance from the headwall to the tip of the streamline at the sidewall

*Graduate Research Assistant, Mechanical, Aerospace and Biomedical Engineering Department. Member AIAA, ASME.
†H. H. Arnold Chair of Excellence in Advanced Propulsion, Mechanical, Aerospace and Biomedical Engineering Department. Associate Fellow AIAA. Fellow ASME.

Subscripts

c	=	choking or centerline conditions
w	=	wall conditions

I. Introduction

ESTIMATING the mean flowfield in porous wall-injecting chambers is vital to the design of solid rocket motors (SRMs). In fact, the mathematical determination of the pressure distribution plays a key role in prescribing the stress loads on the propellant grain, insulation, and rocket frame. From a modeling perspective, the pressure field remains of paramount importance to studies concerned with predicting acoustic instability, understanding the onset of erosive burning, and assessing hydrodynamic stability factors. In this context, Culick[1] developed an incompressible mean flow solution that became widely accepted in the aerospace community. In his 1966 work, Culick[1] considers an internally burning cylinder and recovers the cosine–shaped velocity profile suggested a decade earlier by Taylor.[2] Extending this problem to the compressible context, investigations by two notable groups, Dunlap, Willoughby and Hermsen,[3] and Traineau, Hervat and Kuentzmann,[4] reported rich characteristics of the spatially developing motion as it was shown to exhibit appreciable steepening beyond the Taylor-Culick baseline.[1,2] Such departure from the incompressible approximation was confirmed to have a substantial bearing on the hydrodynamic instability investigation of a simulated rocket motor. As shown by Venugopal,[5,6] a small change in the mean flow can be substantially magnified in the unsteady, compressible flow simulation. These observations were further supported by numerical simulations attributed to Beddini,[7] Baum, Levine and Lovine,[8] Liou and Lien,[9] and Apte and Yang,[10,11] among others.

In this article, we derive an explicit solution to the compressible axisymmetric flow analog. Among the analytical techniques used in this context are the Rayleigh-Janzen and Prandtl–Glauert expansion methods.[12] The latter consists of perturbing the velocities in terms of a shape parameter first, and then treating the reduced equations using traditional approaches. A variant of this technique was pursued by Traineau, Hervat and Kuentzmann[4] whose work was revisited by Balakrishnan, Liñan and Williams.[13] Their analytical efforts relied on scaling arguments to justify the dismissal of the radial momentum equation, thereby reducing the remaining axial momentum, mass, energy, ideal gas, and isentropic state relations to a single integral expression. In a follow-up study,[14] they related the mass flux to the pressure response through St. Robert's power law.

Another analytical technique in relation to this problem consists of a variant of the Rayleigh–Janzen perturbation expansion.[15,16] First applied by Majdalani[17] in the treatment of the axisymmetric porous cylinder and by Maicke and Majdalani[18] in the planar flow analog, the method consists of expanding the compressible equations of motion in the square of the wall injection Mach number. These researchers derived a closed–form approximation to the fully two-dimensional or axisymmetric compressible flowfields. Moreover, their efforts led to the identification of the sonic distance as the appropriate lengthscale for normalization; when inserted into one-, two-, or three-dimensional solutions, it would promote a self-similar, parameter-independent behavior of the results for all wall Mach numbers.

The present investigation builds on the work by Traineau, Hervat and Kuentzmann,[4] Balakrishnan, Liñan and Williams,[13] and Akiki and Majdalani.[19,20] Using an Abel inversion, the integral formulation developed previously is solved analytically for integer values of $1/(\gamma-1)$ and three injection configurations. These correspond to constant mass flux, constant injection speed, and spatially oscillatory injection speed. The latter will be introduced and explored given its relevance to the modeling of erosive burning of solid propellants.[21,22] Granted these three injection patterns, our objective will be to provide analytical solutions for the pressure distribution inside a compressible, axisymmetric porous cylinder, such as the one used to represent an idealized SRM.

II. Mathematical Model

A. Geometry

A solid rocket motor can be modeled as a slender, elongated tube with sidewall injection. In this article, we consider the injection driven flow of an ideal gas in a cylinder of radius a and length L_0 such that $a << L_0$. As shown in Fig. 1a, the sidewalls are porous, allowing gas to be injected inwardly at a velocity $U_w(x)$. Figure 1b shows the origin of the coordinate system located at the center of the inert headwall. The downstream end is left open to the atmosphere, hence simulating a nozzeless rocket engine.

B. Formulation

Under the assumption of low chamber aspect ratio, $a/L_0 << 1$, the system's conservation equations may be conveniently expressed as:

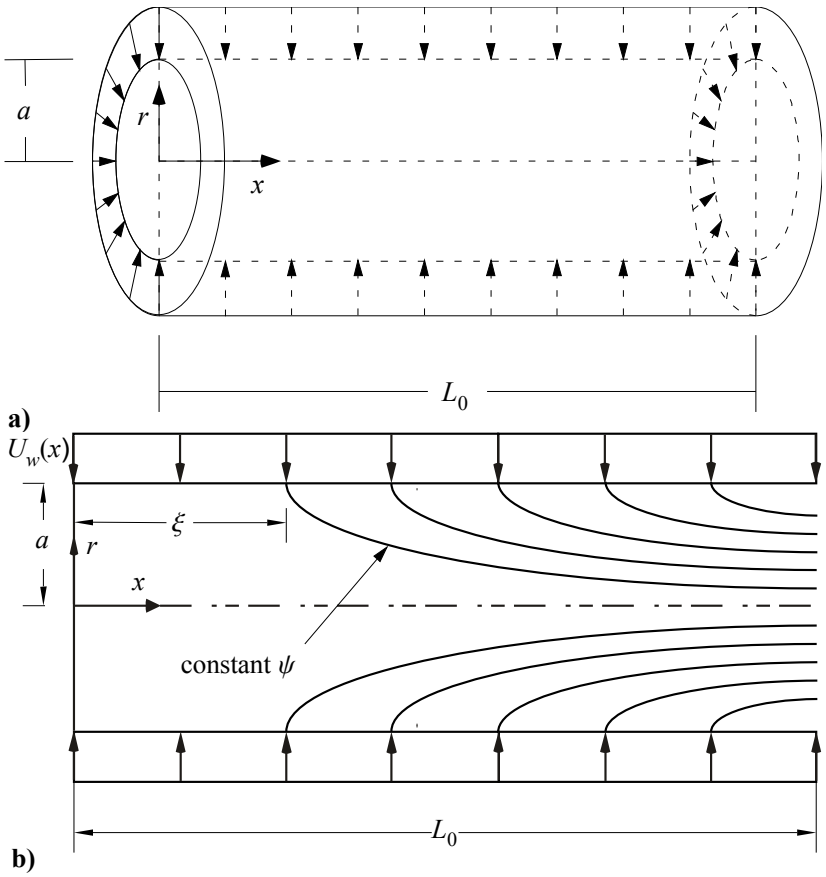

Figure 1. Schematic diagram of a slender porous chamber.

$$\frac{\partial(\rho u r)}{\partial x}+\frac{\partial(\rho v r)}{\partial r}=0 \text{ (compressible continuity)} \tag{1}$$

$$\rho u\frac{\partial u}{\partial x}+\rho v\frac{\partial u}{\partial r}=-\frac{\partial p}{\partial x} \text{ (axial momentum)} \tag{2}$$

$$\frac{\partial p}{\partial r}=0 \text{ (radial momentum)} \tag{3}$$

and

$$\rho u\frac{\partial}{\partial x}\left(c_pT+\frac{u^2}{2}\right)+\rho v\frac{\partial}{\partial r}\left(c_pT+\frac{u^2}{2}\right)=0 \text{ (energy)} \tag{4}$$

Furthermore, the gas may be assumed to be ideal with a constant c_p such that

$$p=\frac{\gamma-1}{\gamma}c_p\rho T \text{ (ideal gas)} \tag{5}$$

Following the integral framework described previously,[13,19] the governing equations can be reduced to

$$\sqrt{\frac{\gamma}{\gamma-1}}=2\int_0^X\left[P(\Xi)\right]^{n-1}\left[\frac{P(\Xi)}{P(X)}\right]^{1/\gamma}\left[1-\left(\frac{P(X)}{P(\Xi)}\right)^{(\gamma-1)/\gamma}\right]^{-1/2}\mathrm{d}\Xi \tag{6}$$

Equation (6) is an integral equation relating the pressure and the axial distance; once solved, it will provide the pressure distribution needed to extract the temperatures, velocities and Mach numbers in the two-dimensional, axisymmetric domain.

III. Exact Solution Using the Abel Transform

The Abel transformation exists between two functions $f(s)$ and $g(t)$ given a parameter α such that $0<\alpha<1$. Then considering the definite integral

$$f(s)=\int_0^s \frac{g(t)}{(s-t)^{\alpha}}\,\mathrm{d}t \tag{7}$$

its Abel inversion yields:

$$g(t)=\frac{\sin(\pi\alpha)}{\pi}\frac{\mathrm{d}}{\mathrm{d}t}\int_0^t \frac{f(s)\mathrm{d}s}{(t-s)^{1-\alpha}} \tag{8}$$

In order to make use of this formulation, we first rearrange Eq. (6) into

$$P(X)^{1/\gamma}=\int_1^{P(\Xi)} \frac{2\sqrt{\dfrac{\gamma}{\gamma-1}}P(\Xi)^{\gamma+3/2\gamma}\,P(\Xi)^{n-1}}{\sqrt{P(\Xi)^{(\gamma-1)/\gamma}-P(X)^{(\gamma-1)/\gamma}}}\left[-\frac{\mathrm{d}\Xi}{\mathrm{d}P(\Xi)}\right]\mathrm{d}P \tag{9}$$

A dual variable transformation in s and t is then inserted into Eq. (9) with the aim of converting it into a form that conforms to Eq. (7). Starting with

$$s=1-P(X)^{\frac{\gamma-1}{\gamma}},\quad t=1-P(\Xi)^{\frac{\gamma-1}{\gamma}} \tag{10}$$

We substitute back into Eq. (9) and simplify. This enables us to identify:

$$f(s)=P(X)^{1/\gamma}\qquad\text{and}\qquad g(t)=-2\sqrt{\frac{\gamma}{\gamma-1}}P(\Xi)^{\gamma+3/2\gamma}\,P(\Xi)^{n-1}\frac{\mathrm{d}\Xi}{\mathrm{d}P(\Xi)} \tag{11}$$

Their backward substitution into Eq. (9) leaves us with

$$g(t)=\frac{1}{\pi}\frac{\mathrm{d}}{\mathrm{d}t}\int_0^t \frac{(1-s)^{1/(\gamma-1)}}{\sqrt{t-s}}\mathrm{d}s \tag{12}$$

Equation (12) can be readily integrated for integer values of $1/(\gamma-1)$. The list of ratios of specific heats with physical significance includes 1.5, 1.33, 1.25, 1.2, 1.17, 1.14, 1.125 and 1.11. For the purpose of demonstration, the analysis is detailed for $\gamma=1.5$; however, the remaining solutions can be extracted from a recursive formula that will be later discussed. Evaluating the integral in Eq. (12), one gets

$$\frac{\mathrm{d}\Xi}{\mathrm{d}P(\Xi)}=\frac{\left[-8P(\Xi)^{2/3}+4P(\Xi)^{1/3}+1\right]P(\Xi)^{-n-1/2}}{6\pi\sqrt{3-3P(\Xi)^{1/3}}} \tag{13}$$

Knowing that the pressure is assumed one-dimensional, and that Ξ represents an axial distance, it is appropriate to replace Ξ with the axial coordinate. Subsequent integration of Eq. (13) renders:

For $n=0$

$$X=\frac{\sqrt{1-P^{1/3}}\left(8P^{2/3}+4P^{1/3}+3\right)P^{1/6}-3\sin^{-1}\left(P^{1/6}\right)}{6\sqrt{3}\pi}+C_1 \tag{14}$$

For $n=1$

$$X=-\frac{\left[\sqrt{1-P^{1/3}}\left(14P^{1/3}+1\right)+24\sqrt{P}\sin^{-1}\left(P^{1/6}\right)\right]}{3\sqrt{3}\sqrt{P}\pi}+C_2 \tag{15}$$

At this point, the boundary at the headwall can be used to specify the constants $C_1=1/4\sqrt{3}$ and $C_2=4/\sqrt{3}$. Note that Eqs. (14) and (15) are exact solutions of the governing integral equation for the case of $\gamma=1.5$. A recursive relation may be developed to extract the expressions relating the pressure and the axial distance for different values of γ. After much effort, we find, for $n=0$, the exact relation:

$$X=\left[\left(\prod_{l=0}^{k-1}\frac{2l+2}{2l+1}\right)\frac{\sqrt{1-P^{\frac{1}{k+1}}}}{\sqrt{k+1}}\sum_{m=0}^{k}\left(P^{\frac{m}{k+1}}\right)\prod_{l=0}^{k-m-1}\frac{2l+1}{2l+2}\right]\frac{P^{\frac{1}{2(k+1)}}}{2\pi}-\frac{\arcsin P^{\frac{1}{2(k+1)}}}{2\sqrt{k+1}\pi}+\frac{1}{4\sqrt{k+1}} \tag{16}$$

where $k\equiv 1/(\gamma-1)$, with integer values of k between 2 and 10 ($1.1\le\gamma\le 1.5$). For the particular case of $n=1$, the corresponding list of exact solutions is cataloged in Table 1. Equation (16) represents the one-dimensional pressure distribution as a function of the axial distance. Its range of applicability ends at the point where choking occurs, and

Table 1. Exact solutions of the pressure distribution in a simulated SRM for different ratios of the specific heats

γ	$X(P)$
$n=0$ (constant injection mass flux)	
$\left[\frac{3}{2},\frac{10}{9}\right]$	$\frac{1}{2}\frac{P^{\frac{1}{2(k+1)}}}{\pi}\left(\prod_{l=0}^{k-1}\frac{2l+2}{2l+1}\right)\frac{\sqrt{1-P^{\frac{1}{k+1}}}}{\sqrt{k+1}}\sum_{m=0}^{k}P^{\frac{m}{k+1}}\left(\prod_{l=0}^{k-m-1}\frac{2l+1}{2l+2}\right)-\frac{\arcsin P^{\frac{1}{2(k+1)}}}{2\pi\sqrt{k+1}}+\frac{1}{4\sqrt{k+1}}$
$n=1$ (constant injection velocity)	
$\frac{3}{2}$	$-\frac{1}{3\pi\sqrt{3P}}\left[(1+14P^{1/3})\sqrt{1-P^{1/3}}-24\sqrt{P}\arccos(P^{1/6})\right]$
$\frac{4}{3}$	$-\frac{2}{75\pi P^{5/8}}\left[\left(3+14P^{1/4}+148\sqrt{P}\right)\sqrt{1-P^{1/4}}-240P^{5/8}\arccos(P^{1/8})\right]$
$\frac{5}{4}$	$-\frac{1}{735\pi\sqrt{5}P^{7/10}}\left[(75+258P^{1/5}+904P^{2/5}+8528P^{3/5})\sqrt{1-P^{1/5}}-13,440P^{7/10}\arccos(P^{1/10})\right]$
$\frac{6}{5}$	$-\frac{\sqrt{2/3}}{6615\pi P^{3/4}}\left[(245+730P^{1/6}+1884P^{1/3}+5872\sqrt{P}+52,064P^{2/3})\sqrt{1-P^{1/6}}-80,640P^{3/4}\arccos(P^{1/12})\right]$
$\frac{7}{6}$	$-\frac{1}{114,345\pi\sqrt{7}P^{11/14}}\left[(6615+18,130P^{1/7}+40,520P^{2/7}+92,976P^{3/7}+271,808P^{4/7}\right.$ $\left.+2,317,696P^{5/7})\sqrt{1-P^{1/7}}-3,548,160P^{11/14}\arccos(P^{1/14})\right]$
$\frac{8}{7}$	$-\frac{2\sqrt{2}}{19,324,305\pi P^{13/16}}\left[(114,345+296,730P^{1/8}+609,980P^{1/4}+1,211,920P^{3/8}\right.$ $+2,607,456\sqrt{P}+7,320,448P^{5/8}+60,766,976P^{3/4})\sqrt{1-P^{1/8}}$ $\left.-92,252,160P^{13/16}\arccos(P^{1/16})\right]$
$\frac{9}{8}$	$-\frac{1}{96,621,525\pi P^{5/6}}\left[(1,288,287+3,216,906P^{1/9}+6,261,192P^{2/9}+11,441,360P^{1/3}\right.$ $+21,312,640P^{4/9}+44,025,600P^{5/9}+120,202,240P^{2/3}$ $\left.+978,421,760P^{7/9})\sqrt{1-P^{1/9}}-1,476,034,560P^{5/6}\arccos(P^{1/18})\right]$
$\frac{10}{9}$	$-\frac{\sqrt{2/5}}{1,861,574,715\pi P^{17/20}}[(32,207,175+78,156,078P^{1/10}+146,371,764P^{1/5}+253,240,848P^{3/10}$ $+433,851,040P^{2/5}+775,880,960\sqrt{P}+1,558,371,840P^{3/5}$ $+4,168,878,080P^{7/10}+33,430,343,680P^{4/5})\sqrt{1-P^{1/10}}$ $-50,185,175,040P^{17/20}\arccos(P^{1/20})]$

this is accompanied by $\mathrm{d}P/\mathrm{d}X\to\infty$, a condition that enables us to calculate the critical distance. It may be instructive to that note the exact representations in Eq. (16) and Table 1 have been carefully verified through comparisons to the numerical solution of Eq. (6); in all test cases, the analytical predictions coincided with the numerical results. In the interest of brevity, the attendant discussion is omitted here.

With the pressure distribution in hand, one can sample the data and solve for the radial distance numerically using

$$\left(\frac{r}{a}\right)^2=2\sqrt{\frac{\gamma-1}{\gamma}}\int_0^{\Xi}\left[P(\Xi')\right]^{n-1}\left[\frac{P(\Xi')}{P(X)}\right]^{1/\gamma}\left[1-\left(\frac{P(X)}{P(\Xi')}\right)^{(\gamma-1)/\gamma}\right]^{-1/2}\mathrm{d}\Xi' \tag{17}$$

where all quantities on the right-hand-side are known. Subsequently, the temperature can be extracted from the isentropic relation,

$$T(x,\xi)/\left[p(x)\right]^{(\gamma-1)/\gamma} = T_w(\xi)/\left[p(\xi)\right]^{(\gamma-1)/\gamma} \tag{18}$$

Having the temperature, one can solve for the velocity profile using the relation derived from the energy equation,

$$T(x,\xi)+u^2(x,\xi)/(2c_p) = T_w(\xi) \quad \text{or} \quad u(x,\xi) = \sqrt{2c_p\left[T_w(\xi)-T(x,\xi)\right]} \tag{19}$$

For the calculation of the Mach number, one can employ the compressible flow relation $M = u/\sqrt{(\gamma-1)c_pT}$ to retrieve

$$M = \sqrt{\left(\frac{2}{\gamma-1}\right)\left[\frac{T_w(\xi)}{T(x,\xi)}-1\right]} = \sqrt{\left(\frac{2}{\gamma-1}\right)\left[\left(\frac{P(\Xi)}{P(X)}\right)^{(\gamma-1)/\gamma}-1\right]} \tag{20}$$

At this juncture, most of the parameters characterizing the flow are available.

IV. Results and Discussion

By way of verification, we turn our attention to two analytical studies of the compressible flowfield in porous chambers. The first is by Majdalani[17] who developed a closed-form solution for the problem. In his work, perturbations methods are used with a variant of the Rayleigh-Janzen expansion. His approach, based on a small characteristic wall Mach number, has been shown to provide a suitable gaseous flow representation for rocket motor applications. Majdalani's model is herein summarized for a flow driven by a uniform speed at the injecting sidewall:

$$\psi = M_w\psi_0\left(1-\tfrac{1}{4}\Gamma^2\left[1+\tfrac{1}{3}\cos(\pi r^2)\right]\chi^2+\tfrac{1}{2}M_w^2\right) \text{ (streamfunction)} \tag{21}$$

where $\psi_0 = x\sin(\frac{1}{2}\pi r^2)$ and $\chi = x/L_s$; other parameters include

$$M_c = \Gamma\chi\frac{2+\frac{1}{3}\Gamma^2\chi^2-M_w^2}{\sqrt{4-2(\gamma-1)\Gamma^2\chi^2}}; \text{ (centerline Mach number)} \tag{22}$$

$$p_c = 1-\tfrac{1}{2}\gamma\Gamma^2\chi^2(1-M_w^2)-\tfrac{1}{24}\gamma\Gamma^4\chi^4 \text{ (centerline pressure)} \tag{23}$$

$$T_c = 1-\tfrac{1}{2}(\gamma-1)\Gamma^2\chi^2(1-M_w^2)-\tfrac{1}{6}(\gamma-1)\Gamma^4\chi^4 \text{ (centerline temperature)} \tag{24}$$

where the sonic length, L_s, is related to the Γ function through

$$\Gamma \equiv \pi M_w L_s = \sqrt{\lambda-2\gamma-2+2(2\gamma^2+\gamma-1)/\lambda} \tag{25}$$

where

$$\lambda = \left(28+12\gamma-6\gamma^2-8\gamma^3+6\sqrt{22+18\gamma-6\gamma^2-14\gamma^3-3\gamma^4}\right)^{1/3} \tag{26}$$

or, in expanded form,

$$\Gamma \cong 0.884622-0.177299(\gamma-1)+0.0539119(\gamma-1)^2-0.0180615(\gamma-1)^3 \tag{27}$$

Another solution of relevance is a one-dimensional model referenced recently by Gany and Aharon.[23] Unlike Majdalani's constant injection velocity, their basic isentropic model assumes a uniform mass flux along the sidewall. In the interest of clarity, their key thermodynamics variables are given by

$$M_{1D} = \sqrt{\frac{1-\sqrt{1-\chi^2}}{1+\gamma\sqrt{1-\chi^2}}} \tag{28}$$

$$P_{1D} = (1+\gamma)^{-1}\left(1+\gamma\sqrt{1-\chi^2}\right) \tag{29}$$

and

$$T_{1D} = (1+\gamma)^{1/\gamma-1}\left(1+\gamma\sqrt{1-\chi^2}\right)^{1-1/\gamma} \tag{30}$$

Traditionally, the critical distance, also known as the sonic length, represents the distance from the headwall to the point at which the Mach number reaches unity. The reason that a critical point is used in the definition of L_s can be attributed to compressible flow theory being mostly developed in a one-dimensional setting. In the present work, the problem is two-dimensional, and the Mach number reaches sonic conditions along a bell-shaped curve rather than a point. To reconcile with one-dimensional predictions wherein values are essentially area-averaged at a given

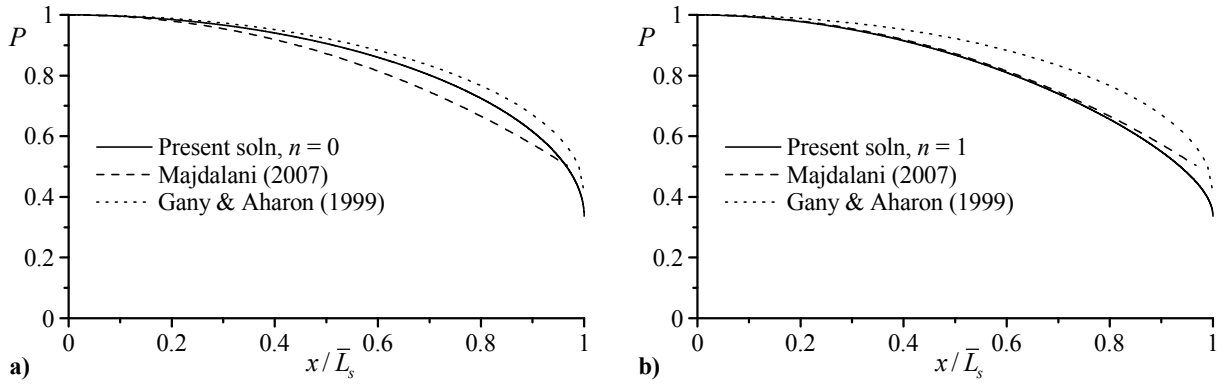

Figure 2. Comparison between the present semi-analytical formulation and both 1D and 2D solutions by Gany & Aharon (1999) and Majdalani (2007), respectively. The present solution is featured for a) constant mass flux (n = 0) and b) constant wall injection speed (n = 1).

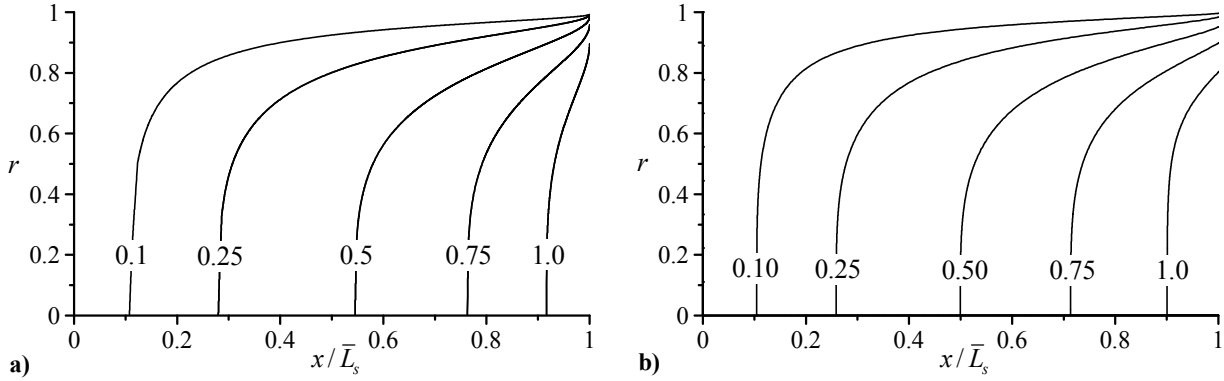

Figure 3. Local Mach number contours according to a) numerical integration, and b) analytical solution by Majdalani (2007).

axial station, a new definition is warranted, namely, that of an area-averaged critical length, $\bar{L}_s$. Accordingly, a cross-section will be fully choked when the local average Mach number reaches unity.

In what follows, results of the present solution are compared to the two analytical models discussed earlier. Figure 2 shows the pressure distribution in the chamber pursuant to Eq. (16). Because the two models are derived under slightly different boundary conditions at the sidewall, we present two sets of comparisons for a) $n = 0$ and b) $n = 1$. The comparison reflects a qualitative agreement with the one-dimensional model. The minor discrepancy observed on this graph can be linked to the additional contributions brought about by two-dimensionality. As for Fig. 2b, we note an excellent agreement with Majdalani's solution,[17] except for the part close to the choking region. Therein, the present solution exhibits a steeper slope as it approaches the sonic point. This may be attributed to the fundamental assumptions used at the forefront of these two dissimilar formulations. In Majdalani's derivation, the pressure, temperature and density parameters are non-dimensionalized with respect to their reference conditions at the headwall. By so doing, their analysis implies constant entropy along the length of the injecting wall; in the present framework, entropy is held constant along a streamline but varied along the sidewall. These conditions give rise to the cases of homentropic versus isentropic flow. With the understanding that turbulence and viscous stresses become significant near the critical length, dissimilarities that may be connected with entropy distribution and reversibility assumptions become magnified in the vicinity of the choking section.

In order to map the Mach number throughout the domain, Eq. (20) may be used to calculate the resulting M everywhere. Forthwith, iso-Mach number contour lines are provided in Fig. 3 using a) numerical integration and b) analytical predictions based on Majdalani's model.[17] Despite the slight dissimilarity in their contour curvatures near choking (upper rightmost corner), the two models appear to display visible agreement in their Mach number predictions elsewhere. Furthermore, the location of the $M = 1$ condition in both models is realized along a two-

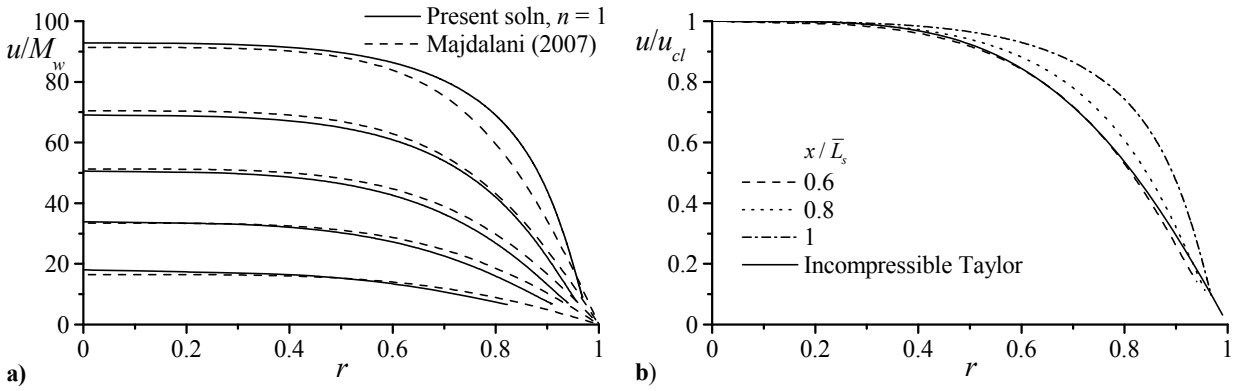

Figure 4. Part a) displays the spatial evolution of the axial velocity for $M_w = 0.01$ at $x/\bar{L}_s = 0.2$, 0.4, 0.6, 0.8 and 1. Part b) depicts the steepening of the velocity profiles relative to the incompressible solution by Taylor (1956).

dimensional axisymmetric surface in lieu of a point. This is due to the contours for $M = 1$ in Fig. 3 being lines of revolution about the chamber axis.

As far as the main velocity is concerned, the evolution of the axial speed is displayed in Fig. 4a and compared to Majdalani's model. Results are shown at evenly spaced intervals of $x/\bar{L}_s = 0.2, 0.4, \ldots, 1$. The profiles appear to be in agreement except in the choking region where the present solution exhibits a blunter profile. Compared to the incompressible Taylor solution shown in Fig. 4b, our velocities taken at several axial stations develop into a blunter, turbulent-like profile. These compressibility effects are consistent with those reported using various other techniques by Majdalani,[17] Maicke and Majdalani,[18] Traineau, Hervat and Kuentzmann,[4] Balakrishnan, Liñan and Williams,[14] Apte and Yang,[11] and others.

V. Flowfield Driven by Oscillatory Injection

Having validated the present formulation, its ability to accommodate various injection profiles can be immediately tested. Originally, the solution is developed for a propellant burning rate behavior that follows St. Robert's power law. However, in modeling erosive burning of propellants, it is useful to explore the effects of varying the velocity profile along the injecting surface.[21,22] This may be accomplished by first nondimensionalizing the variables $P(X)$, X and Ξ with no pressure dependency. For this, we let:

$$P(X) = \frac{p(x)}{p_0} \tag{31}$$

$$X = \sqrt{\frac{\gamma}{\gamma-1}}\frac{1}{a}\int_0^x \frac{U_w(x')}{\sqrt{2c_pT_w(x')}}\mathrm{d}x' \tag{32}$$

and

$$\Xi = \sqrt{\frac{\gamma}{\gamma-1}}\frac{1}{a}\int_0^\xi \frac{U_w(x')}{\sqrt{2c_pT_w(x')}}\mathrm{d}x' \tag{33}$$

Whereas the normalization of P is straightforward, those of X and Ξ are based on their upper integral bounds. This group of coordinate distortions transform Eqs. (17) and (6) into

$$\left(\frac{r}{a}\right)^2 = 2\sqrt{\frac{\gamma-1}{\gamma}}\int_0^\Xi \left[\frac{P(\Xi')}{P(X)}\right]^{1/\gamma}\left\{1-\left[\frac{P(X)}{P(\Xi')}\right]^{(\gamma-1)/\gamma}\right\}^{-1/2}\mathrm{d}\Xi' \tag{34}$$

and

$$\sqrt{\frac{\gamma}{\gamma-1}} = 2\int_0^X \left[\frac{P(\Xi)}{P(X)}\right]^{1/\gamma}\left\{1-\left[\frac{P(X)}{P(\Xi)}\right]^{(\gamma-1)/\gamma}\right\}^{-1/2}\mathrm{d}\Xi \tag{35}$$

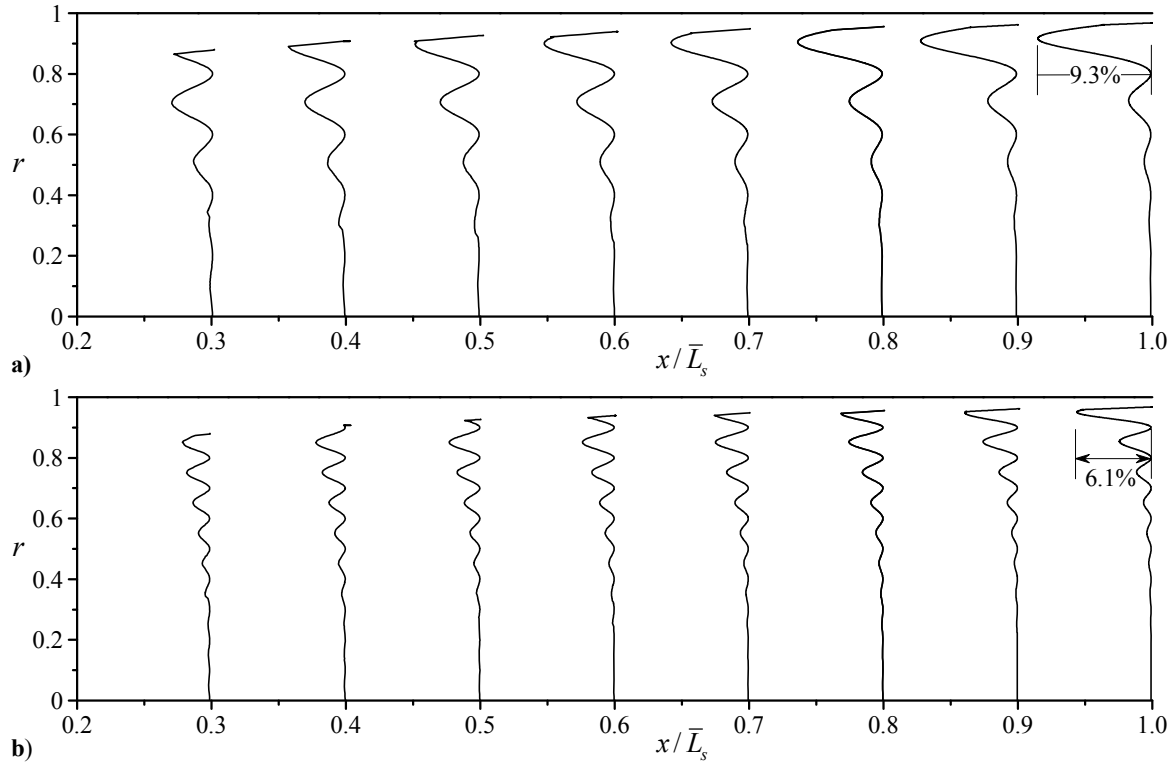

Figure 5. Axial velocity fluctuations due to spatially oscillatory injection using a) η = 5 and b) η = 10. Here α = 0.3 and γ = 1.33.

Equations (34) and (35) can be reproduced from Eqs. (6) and (17) by entirely suppressing the pressure dependency and setting $n = 1$. The explicit solutions associated with this case are already provided in Table 1.

At this stage, an oscillatory velocity profile at the injecting wall may be imposed viz.[21]

$$U_w(x) = U\left[1 + \alpha \sin\left(2\pi\eta \frac{x}{\bar{L}_s}\right)\right] \tag{36}$$

where α and η are parameters controlling the amplitude and number of spatial wavelengths between $x = 0$ and $\bar{L}_s$ (hence commensurate with the spatial wave number). Assuming a constant temperature along the sidewall, Eq. (32) can be integrated given that U and T_w are known quantities that can be calculated from the characteristic wall Mach number. Next, the axial velocity can be determined in terms of x to account for the spatial oscillations. To examine the effect of the propellant burning rate fluctuations on the flow, we start by computing the velocities with an oscillation amplitude of 30% of the blowing speed (i.e., $\alpha = 0.3$). We then subtract the outcome from a flowfield driven by a uniform injection profile (of magnitude U). Results are given in Fig. 5 at different axial locations for a) $\eta = 5$ and b) $\eta = 10$. In this graph, the velocity magnitude is scaled with respect to the centerline velocity; this makes it easier for us to visualize and infer the effects of burning rate fluctuations. Axially, the propagation of disturbances becomes magnified as we move downstream, thus reaching a maximum decrement of 9.3% (at the choking length) for $\eta = 5$ and 6.1% for $\eta = 10$. Conversely, the radial propagation of disturbances originating at the sidewall becomes less pronounced as we move in the downstream direction. Although the amplitude of oscillations is taken to be the same for both cases, higher wave numbers lead to a more rapid attenuation of sidewall disturbances.

One can also study the pressure perturbations arising from this undulating boundary. Figure 6 showcases the pressure fluctuations being subtracted from the flow driven by uniform injection. On the one hand, results show an increase in pressure of up to 9.1% for $\eta = 5$, while, on the other hand, the pressure is decreased by 1.6% for $\eta = 10$. This unpredictable response of the pressure to surface irregularities or propellant burning rate fluctuations warrants further examination. It also explains some of the challenging aspects that must be resolved when predicting for example, erosive or resonant burning behavior.

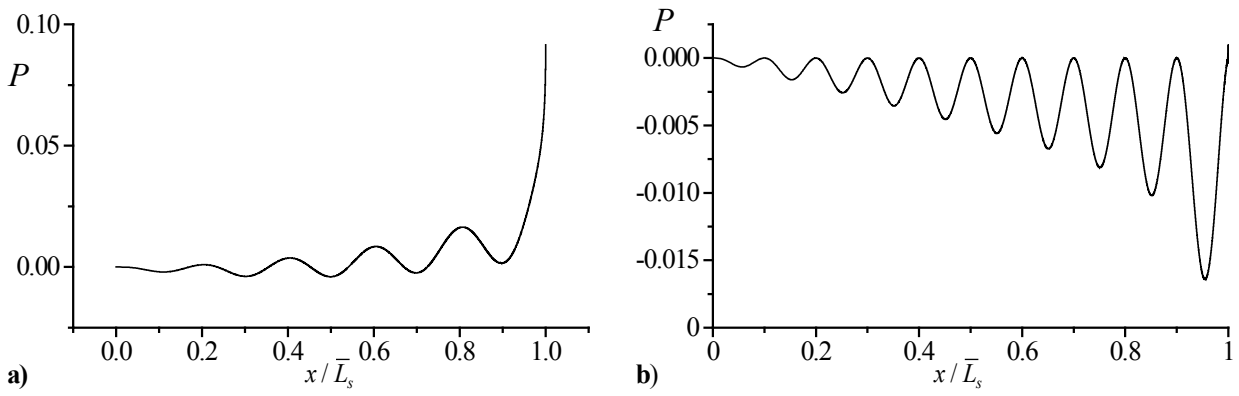

Figure 6. Pressure fluctuations due to spatially oscillatory injection using a) $\eta = 5$ and b) $\eta = 10$. Here $\alpha = 0.3$ and $\gamma = 1.33$.

VI. Conclusions

In this paper, analytical solutions to the integral form of the pressure distribution in a porous cylinder are extracted using an Abel transform. Two sets of exact solutions are retrieved: the first corresponds to a uniformly injecting mass flux and the second to a uniformly injecting velocity. While the former is shown to be reproducible from an explicit recurrence formula, the latter is expressed in series expansions for each viable ratio of specific heats. Results are verified numerically and then compared to other compressible analytical solutions found in the literature, such as those by Majdalani[17] and Gany and Aharon.[23] The present investigation confirms the steepening of velocity profiles and increased gradients at the sidewall due to compressibility. They also confirm the location and shape of the sonic surface of revolution.

Before closing, the unique capability of this framework to accomodate variable surface injection conditions is demonstrated using a spatially oscillatory sidewall velocity. Such behavior may be useful in modeling erosive burning of propellants. At the outset, velocity and pressure fluctuations are extracted and compared for different spatial wave numbers. Our findings indicate that lower wave numbers have a greater impact on the pressure amplitude.

Acknowledgments

This material is based on work supported partly by the National Science Foundation through Grant No. CMMI-0928762, and partly by the University of Tennessee Space Institute, through institutional cost sharing.

References

[1]Culick, F., "Rotational Axisymmetric Mean Flow and Damping of Acoustic Waves in a Solid Propellant Rocket," *AIAA Journal,* Vol. 4, No. 8, 1966, pp. 1462-1464. doi: 10.2514/3.3709

[2]Taylor, G., "Fluid Flow in Regions Bounded by Porous Surfaces," *Proceedings of the Royal Society of London, Series A,* Vol. 234, No. 1199, March 1956, pp. 456-475. doi: 10.1098/rspa.1956.0050

[3]Dunlap, R., Willoughby, P., and Hermsen, R., "Flowfield in the Combustion Chamber of a Solid Propellant Rocket Motor," *AIAA Journal,* Vol. 12, No. 10, 1974, pp. 1440-1445. doi: 10.2514/3.49513

[4]Traineau, J. C., Hervat, P., and Kuentzmann, P., "Cold-Flow Simulation of a Two-Dimensional Nozzleless Solid-Rocket Motor," AIAA Paper 86-1447, July 1986.

[5]Venugopal, P., "Direct Numerical Simulation of Turbulence in a Model Solid Rocket Motor," Ph.D. Dissertation, University of Illinois at Urbana-Champaign, 2003.

[6]Venugopal, P., Moser, R., and Najjar, F., "Direct Numerical Simulation of Turbulence in Injection-Driven Plane Channel Flows," *Physics of Fluids,* Vol. 20, No. 10, 2008, pp. 105103-22. doi: 10.1063/1.2963137

[7]Beddini, R. A., "Injection-Induced Flows in Porous-Walled Ducts," *AIAA Journal,* Vol. 24, No. 11, 1986, pp. 1766-1773. doi: 10.2514/3.9522

[8]Baum, J. D., Levine, J. N., and Lovine, R. L., "Pulsed Instabilities in Rocket Motors: A Comparison between Predictions and Experiments," *Journal of Propulsion and Power,* Vol. 4, No. 4, 1988, pp. 308-316. doi: 10.2514/3.23068

[9]Liou, T., and Lien, W., "Numerical Simulations of Injection-Driven Flows in a Two-Dimensional Nozzleless Solid-Rocket Motor," *Journal of Propulsion and Power,* Vol. 11, No. 4, 1995, pp. 600-606. doi: 10.2514/3.23886
[10]Apte, S., and Yang, V., "Effect of Acoustic Oscillation on Flow Development in a Simulated Nozzleless Rocket Motor," *Solid Propellant Chemistry, Combustion, and Motor Interior Ballistics,* Vol. 185, edited by V. Yang, T. B. Brill, and W.-Z. Ren, AIAA Progress in Astronautics and Aeronautics, Washington, DC, 2000, pp. 791-822.
[11]Apte, S., and Yang, V., "Unsteady Flow Evolution in a Porous Chamber with Surface Mass Injection. Part I: Free Oscillation," *AIAA Journal,* Vol. 39, No. 8, 2001, pp. 1577-1586. doi: 10.2514/2.1483
[12]Shapiro, A. H., *The Dynamics and Thermodynamics of Compressible Fluid Flow*, Vol. 1, The Ronald Press Company, 1953.
[13]Balakrishnan, G., Liñan, A., and Williams, F. A., "Compressible Effects in Thin Channels with Injection," *AIAA Journal,* Vol. 29, No. 12, 1991, pp. 2149-2154. doi: 10.2514/3.10852
[14]Balakrishnan, G., Liñan, A., and Williams, F. A., "Rotational Inviscid Flow in Laterally Burning Solid Propellant Rocket Motors," *Journal of Propulsion and Power,* Vol. 8, No. 6, 1992, pp. 1167-1176. doi: 10.2514/3.11458
[15]Janzen, O., "Beitrag Zu Einer Theorie Der Stationaren Stromung Kompressibler Flussigkeiten (Towards a Theory of Stationary Flow of Compressible Fluids)," *Physikalische Zeitschrift,* Vol. 14, 1913, pp. 639-643.
[16]Rayleigh, L., "On the Flow of Compressible Fluid Past an Obstacle," *Philosophical Magazine,* Vol. 32, No. 187, July 1916, pp. 1-6.
[17]Majdalani, J., "On Steady Rotational High Speed Flows: The Compressible Taylor-Culick Profile," *Proceedings of the Royal Society of London, Series A,* Vol. 463, No. 2077, January 2007, pp. 131-162. doi: 10.1098/rspa.2006.1755
[18]Maicke, B., and Majdalani, J., "On the Rotational Compressible Taylor Flow in Injection-Driven Porous Chambers," *Journal of Fluid Mechanics,* Vol. 603, No. 1, May 2008, pp. 391-411. doi: 10.1017/S0022112008001122
[19]Akiki, M., and Majdalani, J., "Compressibility Effects in Slender Rocket Motors," AIAA Paper 2009-5326, August 2009.
[20]Akiki, M., and Majdalani, J., "Quasi-Analytical Approximation of the Compressible Flow in a Planar Rocket Configuration," AIAA Paper 2010-7080, July 2010.
[21]Zhang, J., and Jackson, T. L., "A Model for Erosive Burning of Homogeneous Propellants," *Combustion and Flame,* Vol. 157, No. 2, 2010, pp. 397-407.
[22]Topalian, V. D., Zhang, J., and Jackson, T. L., "Numerical Study of Erosive Burning in Solid Propellants," AIAA Paper 2010-6903, 2010.
[23]Gany, A., and Aharon, I., "Internal Ballistics Considerations of Nozzleless Rocket Motors," *Journal of Propulsion and Power,* Vol. 15, No. 6, 1999, pp. 866-873. doi: 10.2514/2.5509